Three-body final states in $^{16}O + ^{12}C$-induced reactions: The structure of ^{24}Mg at high excitation*

R. Wieland,† R. Stokstad, A. Gobbi,† D. Shapira, L. Chua, M. W. Sachs, and D. A. Bromley
Wright Nuclear Structure Laboratory, Yale University, New Haven, Connecticut 06520
(Received 3 July 1973)

A kinematically complete study has been made of the $^{12}C + ^{16}O \rightarrow ^{12}C + ^{12}C + \alpha$ and $^{12}C + ^{16}O \rightarrow ^{20}Ne + \alpha + \alpha$ reactions at $E_{^{16}O} = 58.3$ MeV (lab). α particles were detected at a mean laboratory angle of 2°, while the remaining reaction products were observed in coincidence by two large-area position-sensitive detectors placed symmetrically about the beam axis and subtending angles in the range $15° \leq \theta_{lab} \leq 75°$. Particle identification was based on the reaction kinematics. Intense yields to the lowest four states of ^{20}Ne were observed, with a significant fraction thereof proceeding through well defined intermediate states in ^{24}Mg. The predominant interaction in the $^{12}C + ^{12}C + \alpha$ final state appears to involve $^{12}C + \alpha$ corresponding to an excited state at ^{16}O near 10 MeV excitation. No evidence was found for a $^{12}C + ^{12}C$ final state interaction, i.e., for quasimolecular states in ^{24}Mg in the region of excitation $21 \leq E^* \leq 29$ MeV. The predictions of a Hauser-Feshbach statistical model agree rather well with the observed $^{20}Ne + \alpha + \alpha$ yields. A selected portion of the $^{12}C + ^{12}C + \alpha$ yield, not necessarily proceeding through an excited state in ^{16}O, is accounted for by a statistical model assuming formation and decay of compound states in ^{24}Mg.

[NUCLEAR REACTIONS $^{12}C(^{16}O, \alpha_0\alpha_1)^{20}Ne$, $^{12}C(^{16}O, \alpha_0{}^{12}C_1)^{12}C_2$, $E = 58.3$ MeV; measured $\sigma(E\alpha_{0,1}, E_{^{20}Ne}; \theta\alpha_1, \theta_{^{20}Ne})$, $\sigma(E\alpha_0, E_{^{12}C_{1,2}}; \theta_{^{12}C_{1,2}})$, $\theta\alpha_0 = 2°$. Deduced intermediate α-^{12}C interaction; Hauser-Feshbach analysis. Position-sensitive detectors.]

I. INTRODUCTION

The study of nuclear cluster structure in the continuum is a relatively new field in heavy-ion physics and has received much attention in recent years. This activity is related to long-standing questions concerning the distribution of the available energy in a nucleus at high excitation energy: whether this increased energy is sampled statistically by all the individual nucleons in the system, leading to evaporation-like decay, or whether the major fraction of this energy can be absorbed as binding energy in the assembly of simple nuclear subunits, or nuclear clusters involved in simple relative motions. This latter possibility has a long history of conjecture behind it and is especially suited to investigation through heavy-ion-induced reactions, where it becomes possible in principle to transfer or pick up one or more of the clusters through a direct process.

The ^{24}Mg nucleus presents an interesting and challenging subject for the study of cluster phenomena induced via heavy-ion reactions. Figure 1 is an abbreviated level diagram for this system, showing several relevant thresholds. The possibility of cluster-like states appearing in the ^{24}Mg continuum at excitation energies less than 17 MeV was recently raised by the discovery of Middleton, Garrett, and Fortune[1] that a number of very sharp states in ^{24}Mg were selectively populated by the $^{16}O(^{12}C, \alpha)^{24}Mg$ reaction in the energy range 13–17 MeV. In a simple interpretation, this reaction might be considered as the transfer of two or three α particles, either as discrete entities or bound to form ^8Be or ^{12}C, respectively. Arima, Gillet, and Ginocchio[2] had predicted the existence of a number of α-particle, or more generally, "quartet" states in this excitation region: Indicated in Fig. 1 are the positions of the 0^+ members of the lowest quartet configurations predicted in these calculations. Analyses of angular correlations measured in this laboratory[3] and at the University of Pennsylvania[4] have shown that the observed states tend to be of high angular momentum, and it is thus unlikely that they correspond to the quartet states of Ref. 2.

The possibility of cluster configurations in ^{24}Mg at excitation energies in excess of 17 MeV in ^{24}Mg was suggested initially by the observation of nonstatistical resonances in the $^{12}C + ^{12}C$ total reaction cross section by Almqvist, Bromley, and Kuehner[5] and by Patterson, Winkler, and Zaidins.[6] These resonances occurring near the Coulomb barrier ($E^* \approx 20$ MeV) for this channel have been interpreted as ^{12}C-^{12}C molecular configurations.[5] The narrow resonant states observed by Almqvist, Bromley, and Kuehner[5] were found[7] to be of low spin ($I = 0^+, 2^+, 4^+$) and are indicated in Fig. 1. We considered it of interest to pursue this question of heavy clustering through an investigation of the possible existence

of higher-spin molecular configurations at yet higher energies in ^{24}Mg. A preliminary report of the work to be described herein has already appeared.[8] We note further that preliminary results of a similar experiment at Brookhaven National Laboratory have been reported by LeVine, Schwalm, and Littman.[9]

The present experiment was designed to search for heavy-cluster configurations of high spin in ^{24}Mg through direct observation of the decay of these configurations into heavy-cluster components. The known selectivity of the $^{12}C(^{16}O, \alpha)^{24}Mg$ reaction for populating high-spin states in ^{24}Mg was exploited in studying the excitation-energy range $E^* = 20$–30 MeV. A kinematically complete measurement was performed in which α particles, which may populate states in ^{24}Mg, were detected along the beam axis with the resultant decay products of ^{24}Mg observed in two position-sensitive detectors placed at symmetric angles with respect to the beam. Angular distributions resulting from the bombardment of a ^{12}C target by 58.3-MeV ^{16}O ions were obtained as a function of the 0° α-particle energy for the reaction channels ^{20}Ne(g.s., 1.63, 4.25 + 4.91) + α + α, ^{16}O(g.s.) + 2α + α, ^{12}C(g.s.) + ^{12}C + α, and ^{12}C(4.43 MeV) + ^{12}C + α.

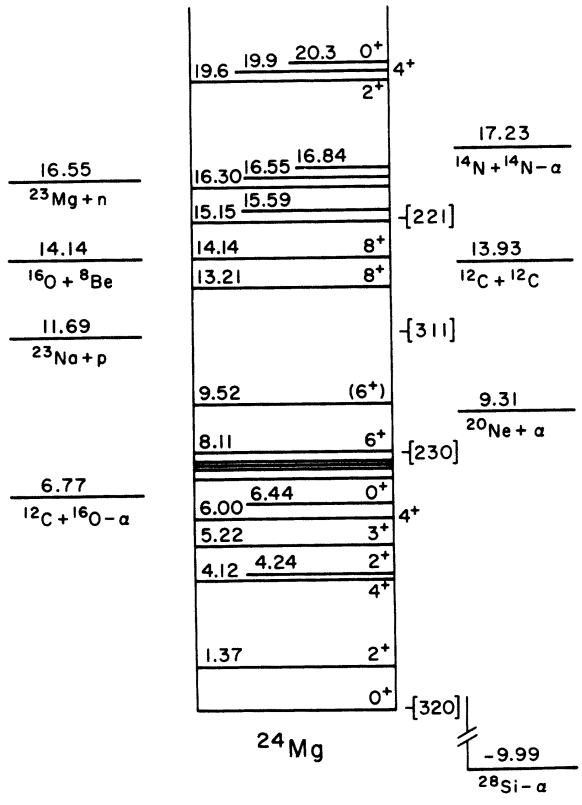

FIG. 1. An abbreviated energy-level diagram for ^{24}Mg. The number of levels (most of which are not shown) increases rapidly above $E^* \sim 10$ MeV. The states indicated between 13 and 17 MeV are those observed in the $^{16}O(^{12}C,\alpha)^{24}Mg$ reaction (Ref. 1), while those near 20 MeV correspond to resonances (Ref. 5) in the $^{12}C + ^{12}C$ reaction.

It was found, as expected from previous measurements on the $^{12}C(^{16}O, \alpha)^{24}Mg(\alpha)^{20}Ne$ reaction,[3,4] that the $^{20}Ne + \alpha + \alpha$ channels carry most (~90%) of the three-body flux at the ^{16}O incident energies studied. An intense α-particle background was found to contribute almost 50% of the observed triple-coincidence yield, and is attributed primarily to the $^{16}O + 3\alpha$ four-body final state in which one particle is undetected. Analyses of the triple-coincidence events provided no evidence, in the excitation range studied, for the existence of *narrow* states in ^{24}Mg having a ^{12}C-^{12}C molecular configuration. Rather, the ^{12}C(g.s.) + ^{12}C(g.s.) + α final state was found to be dominated by a strong final-state interaction between the α particle and a ^{12}C nucleus, occurring at an effective excitation energy of roughly 10 MeV in the ^{16}O compound system.

A statistical model calculation assuming two-stage sequential compound decay was applied to the observed cross sections in the five channels under study; the results show excellent agreement with gross features of the data (for which the above mentioned $^{12}C + ^{12}C + \alpha$ events showing a strong final-state interaction were excluded) both in terms of relative magnitudes and observed excitation energy dependence. This suggests that the fission of ^{24}Mg into two ^{12}C nuclei has been observed, although from decay of a number of broad close-lying levels in ^{24}Mg rather than from long-lived isolated quasimolecular states.

II. EXPERIMENTAL METHOD

Negative ^{16}O ions were produced in a direct-extraction Penning source[10] and accelerated by an MP Van de Graaff accelerator to an energy of 58.3 MeV. The beam was focussed onto a 10-μg/cm^2 carbon target positioned inside a standard 75-cm ORTEC scattering chamber.

The experimental arrangement is shown schematically in Fig. 2. The defining aperture for the beam collimation had a diameter of 1.2 mm. Beam currents on target were restricted to less than 250 nA in order to prevent excessive counting losses.

The detection of light particles at angles near 0° was accomplished by mounting an annular Au-Si surface-barrier detector with a depletion depth of ~700 μm and an area of 300 mm^2 inside a cylindrical aluminum vessel having a 2-mg/cm^2 Havar window and filled with hydrogen gas. The gas pressure corresponded to an absorber thickness of 2.70 mg/cm^2 and was selected to prevent the forward-

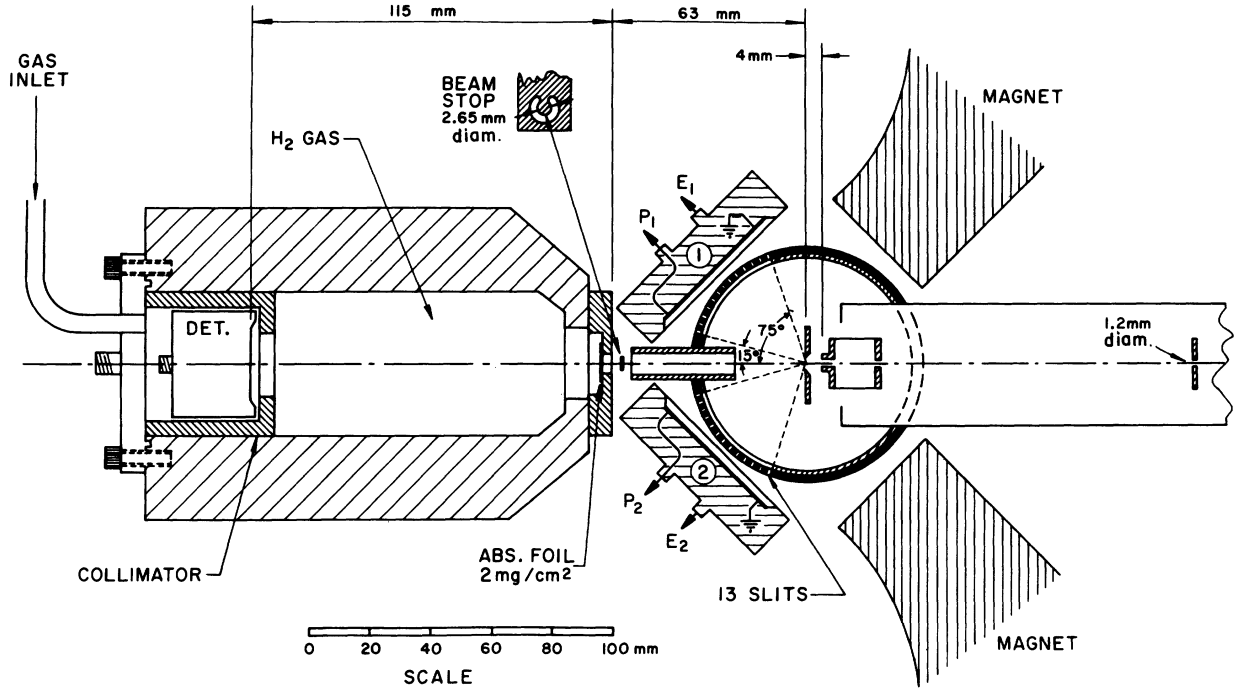

FIG. 2. Schematic diagram of the experimental arrangement. The ring with the 13 slits in front of each position-sensitive detector was used for calibration and was otherwise removed during the data collection.

scattered ^{16}O ions from reaching the detector. A tantalum beam stop 1.5 mm thick and 2.65 mm in diameter was positioned before the Havar window, preventing the direct beam from entering the absorber, and was used during the experiment as a rough monitor of the beam current. This detection system, collimated to subtend 8 msr of solid angle at the target with a mean angle of 2°, possessed several advantages over the system employing metal-foil absorbers used in earlier measurements.[3] First, the hydrogen absorber led to a reduction in the energy straggling of α particles—the resolution improved by nearly a factor of 2 from previous values of $\Delta E = 300$ keV (for a nickel-foil absorber) to $\sim\Delta E = 170$ keV; and second, the thickness of the absorber was continuously and conveniently variable without having to break the chamber vacuum. Direct dE/dx-E particle identification by a counter telescope was not used in the present system. This lack of direct identification did not introduce significant problems in the analysis since the known absorber thickness, known detector depletion depth, and measured kinematic variables of the other decay products were sufficient to eliminate any possible ambiguities.

In addition to the detection of light particles at angles near 0°, two position-sensitive detectors (PSD's), each collimated to an area of 7 mm × 50 mm, were mounted on either side of the beam axis and subtended angles of 15–75° in the laboratory system. Their depletion depth was ~600 μm. Each of these detectors produced two pulses: an energy pulse E and a position-energy pulse PE, where P is proportional to the location along the detector face where the ion was incident. More detailed information on their operation can be found elsewhere.[11] The large magnet indicated in Fig. 2 prevented electrons from the target from reaching the PSD's.

A block diagram of the electronic configuration is shown in Fig. 3. In this system, a triple-coincidence event was defined by the time overlap of two double-coincidence events, the latter arising from coincident particles in the 0° detector and either PSD. Separate double-coincidence events were also accepted for analysis. The gated analog signals for each triple-coincidence event (E_{α_0}, E_{PSD_1}, PE_{PSD_1}, E_{PSD_2}, PE_{PSD_2}, T_{01}, T_{02}) were digitized, processed on line by the Yale IBM nuclear data acquisition system,[12] and simultaneously recorded on magnetic tape for later analysis. The PE/E division was accomplished digitally by software. A five-channel pulser was used to simulate triple-coincidence events. Constant monitoring of the analyzed pulser events revealed no significant variations in gain or in electronic timing during the experiment.

The PSD's were calibrated by means of an annu-

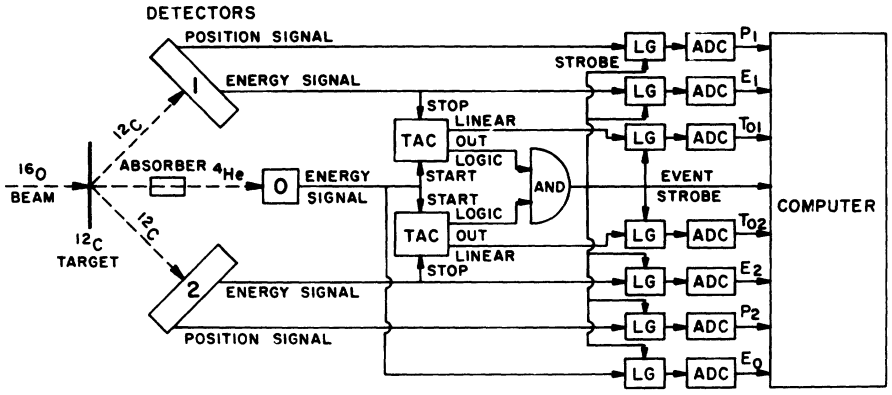

FIG. 3. Block diagram of the electronic configuration used in the triple-coincidence measurement. LG denotes a linear gate.

lar brass ring containing 13 slits covering the angular range of both detectors. For the position calibration, direct noncoincidence measurements were made with the slit system in place using a 58.3-MeV ^{16}O beam incident on a thin vertically mounted gold wire. With this target, scattered ^{16}O ions varying continuously in energy were obtained. A least-squares method was used to determine a 16-parameter transformation from energy channel number and position channel number to absolute laboratory angle.

The energy calibration was determined by accumulating spectra from the elastic scattering of ^{16}O by a 10-$\mu g/cm^2$ thin gold target at three ^{16}O energies: 14.60, 25.24, and 40.52 MeV. A second least-squares analysis resulted in a similar transformation and a calibration in absolute energy. These two transformations were included as part of the final general computer program used in the analysis of the data.

The energy calibration of the 0° detector proceeded in the following way. The energy-loss tables of Northcliffe and Schilling[13] were used to generate a cubic relationship between the energy of the α particle leaving the target and its subsequent lower energy on entering the Si detector after passing through the absorbers. The energy calibration of the Si detector was then determined using this relationship and the identification of known states in ^{24}Mg appearing as peaks in a direct α-particle spectrum.

III. DATA ACQUISITION AND ANALYSIS

A. Acquisition

Data were accumulated over a 200-h period in a series of 27 runs, all of equal integrated-beam current. The total accumulated data consisted of over 11 000 000 double-coincidence and almost 80 000 triple-coincidence events. The triple-coincidence data were analyzed as described in the following subsections.

B. Analyses

The analyses of the triple-coincidence events proceeded in three steps. First a time-correlation ($T_{01} - T_{02}$) analysis of each event was performed to determine its real or random coincidence character. Then a kinematic mass analysis was

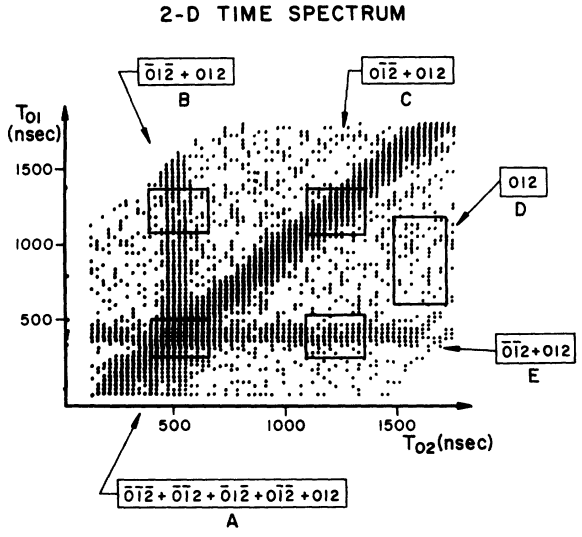

FIG. 4. Two-dimensional time spectrum of the data. Real triple-coincidence events occur in the region where the three lines cross (window A). The time coincidence windows are labeled (0 1 2), where the integers correspond to the labeling of the detectors in Fig. 3. For example, ($\bar{0}$ 1 $\bar{2}$) denotes an event in which the particles observed in detectors 0 and 2 are from the same nuclear collision while the particle observed nearly simultaneously in detector 1 is from an unrelated or random event.

made of the two particles detected in the PSD's, enabling a partial determination of their masses. Final identification was accomplished by determining the total energy or Q value of the event.

1. *Time analysis*

The two-dimensional time-correlation spectrum is shown in Fig. 4. This figure shows three converging loci of events superimposed on a uniform background, representing the four types of random time coincidences that occur in a triple-coincidence measurement. It should be noted that the relatively high intensity of the diagonal line arises from the large kinematic coincidence rate produced by heavy-ion elastic and inelastic two-body scattering. The real triple-coincidence events lie within the region of intersection of these three lines; the subtraction of the random coincidence background was accomplished by defining five two-dimensional windows in the $T_{01} - T_{02}$ parameter subspace as shown in Fig. 4. The designations indicate the type of events enclosed by each window. Those events which occurred in windows A or D were tagged for addition in subsequent pulse-height analyses; those which occurred in B, C, or E were tagged for subtraction. The resulting ratio of real-to-random events in Fig. 4 was 4 to 1. Real-plus-random and random events were subjected to identical analyses, as described below, with the subtraction occurring only at the last stage of the analysis procedure. All of the data presented in the following figures have random events subtracted.

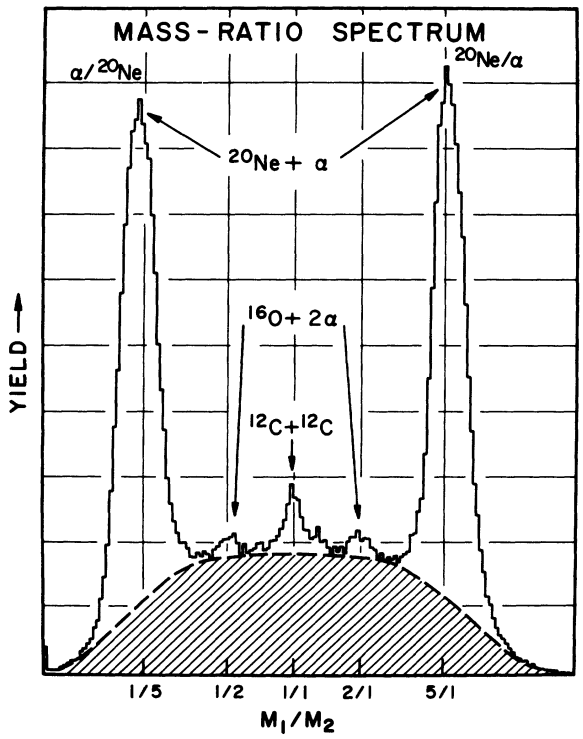

FIG. 5. Mass-ratio spectrum for the particles observed in the position-sensitive detectors. The background area (shaded) was obtained from the two-dimensional mass-ratio–Q_{val} spectrum in Fig. 7. The label $\alpha/^{20}$Ne denoted that events in this peak correspond to the detection of the α particle in PSD_1 and the ^{20}Ne in PSD_2.

2. *Mass-ratio analysis*

The ratio of the masses of the particles incident on the PSD's was determined from the measurement of their energies and angles. The detection of the light particle at 0° results, as a necessary consequence of conservation of linear momentum, in the following expression for the mass ratio:

$$M_1/M_2 = E_2 \sin^2\theta_2 / E_1 \sin^2\theta_1 .$$

Use of this expression is only approximately correct in the present analysis because of the finite solid angle subtended by the 0° detector. A spread in the experimental value of M_1/M_2 is thus introduced. By further assuming that 0° particle to be ^{4}He, a unique identification of the channel can be obtained. Special exceptions to this assumption will be discussed in a later section.

The resulting mass-ratio spectrum is shown in Fig. 5; the large peak at the mass-ratio value $M_1/M_2 = \frac{1}{5}$ corresponds to the detection of an α particle in PSD_1 and a ^{20}Ne in PSD_2 (this peak is labeled as the $\alpha/^{20}$Ne group since it will be necessary to specify in the subsequent discussion which PSD recorded the α particle). Similarly, the peak at $M_1/M_2 = 5$ corresponds to the ^{20}Ne/α group of events where the α particle has been detected in PSD_2. The smaller peak at unity corresponds to the observation of a ^{12}C-^{12}C pair. The smaller peaks at $M_1/M_2 = \frac{1}{2}$, 2 indicate observation of ^{16}O in one PSD and two coincident α particles in the other. The background arises principally from triple-coincidence events corresponding to a four-body final state with one particle going undetected. Much of this background is eliminated by subsequent steps in the analysis. This will be discussed further in the following subsection.

3. *Q-value analysis*

In order to specify uniquely the internal excitation energies in the channel in question, and in order to check on the assumption that an α-particle was indeed detected at 0°, the experimental energy sum

$$Q_{val} = E_0 + E_1 + E_2 = 58.3 + Q$$

was obtained. The resulting spectrum is shown in Fig. 6. The labeled arrows denote, for the respec-

tive mass ratios indicated, the predicted positions of the excited and ground states of the channel based on the summation of the experimentally determined energies of each of the three particles using the absolute energy calibration of the three detectors.

It is also useful to consider the two-dimensional M-Q_{val} spectrum, shown in Fig. 7, for which the one-dimensional mass ratio (Fig. 5) and Q-value spectra (Fig. 6) are projections along the ordinate and abscissa, respectively. Lower and upper discriminator levels of 48 and 281 counts, respectively, have been applied to the computer display from which this figure is taken directly. Several features of the two-dimensional spectrum (Fig. 7) are to be noted. First, the resolution of the $^{20}Ne/\alpha$ group is superior to that of the $\alpha/^{20}Ne$ group. Second, a locus of background events contained by the two curves labeled a is seen to extend approximately from each $\alpha + \alpha + ^{20}Ne$ group into the region of the $^{12}C + ^{12}C^* + \alpha$ group. This will be discussed in Subsec. 4.

The first effect mentioned above was investigated and found to arise from inferior intrinsic energy resolution in PSD_1. It was possible, however, to effect an improved final-state separation in the $\alpha_0 + \alpha_1 + ^{20}Ne$ channel by a consideration of the summed energy as a function of the observed angle of the α particle. Figure 8 shows the resulting spectra whereby the measured energy of the ^{20}Ne has been replaced by a value computed from the known kinematic variables associated with the other two α particles. Subsequent analyses of the events in this channel were done by defining two-dimensional windows about the loci of events associated with each state in ^{20}Ne.

It is apparent from Fig. 8 that nonlinearities in the detection system were not removed completely by the calibration procedure, particularly in the case of PSD_1. The following sources of error in the calibration were investigated. First, the differing dE/dx for α particles, ^{12}C, ^{16}O, and ^{20}Ne ions[13] in the dead layer on the surface of the PSD was considered; it was found that no differential energy variations in excess of 100 keV could be expected from this source. Second, the possibili-

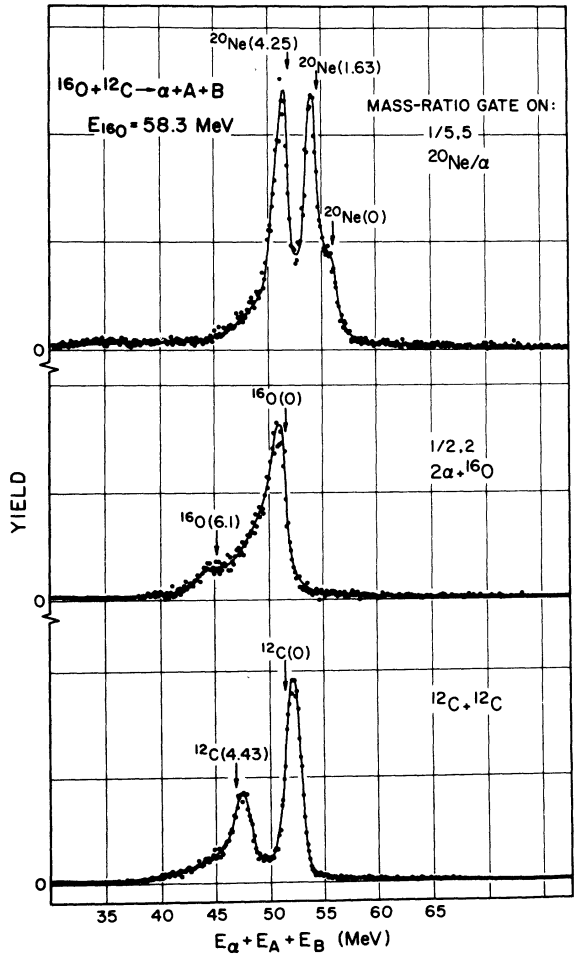

FIG. 6. Q-value spectra for the various three-body channels indicated. The arrows indicate predicted peak positions for the states shown based on the absolute energy calibrations for the three detectors.

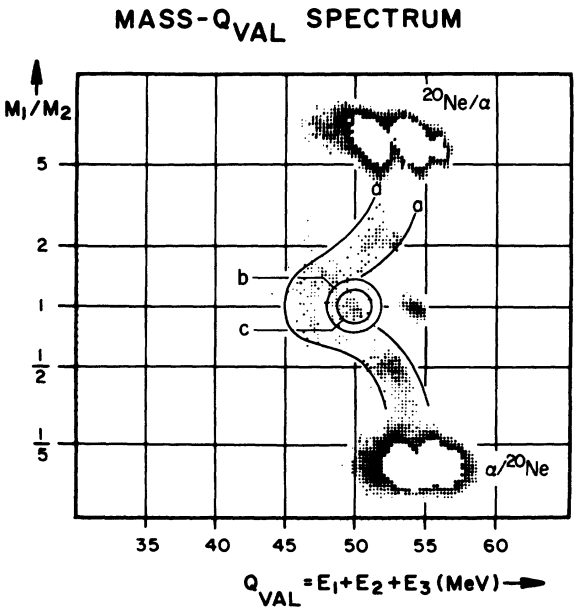

FIG. 7. Two-dimensional spectrum of mass ratio vs Q_{val}. A display window having upper and lower levels of 48 and 281 counts, respectively, is in effect here. Figures 5 and 6 are one-dimensional projections of events in this parameter space. The full curves labeled a, b, and c denote background regions as described in the text.

ty of significant errors introduced through effects of pulse-height defects were considered and discounted largely on the basis of previous studies[14] of these effects for heavy ions stopping in position-sensitive detectors.

Thus, although the different nonlinearities shown in Fig. 8 are not yet completely understood, it should be emphasized that they are sufficiently small (note the suppressed zero on the ordinate) to be of no consequence in the identification of the different particle species in the exit channels; in consequence they do not affect the conclusions of this work. Since the energy spacings of the ground and first excited states of ^{16}O and ^{12}C are much larger than in ^{20}Ne, extended analyses such as those described above were not required for the separation of states in these other channels.

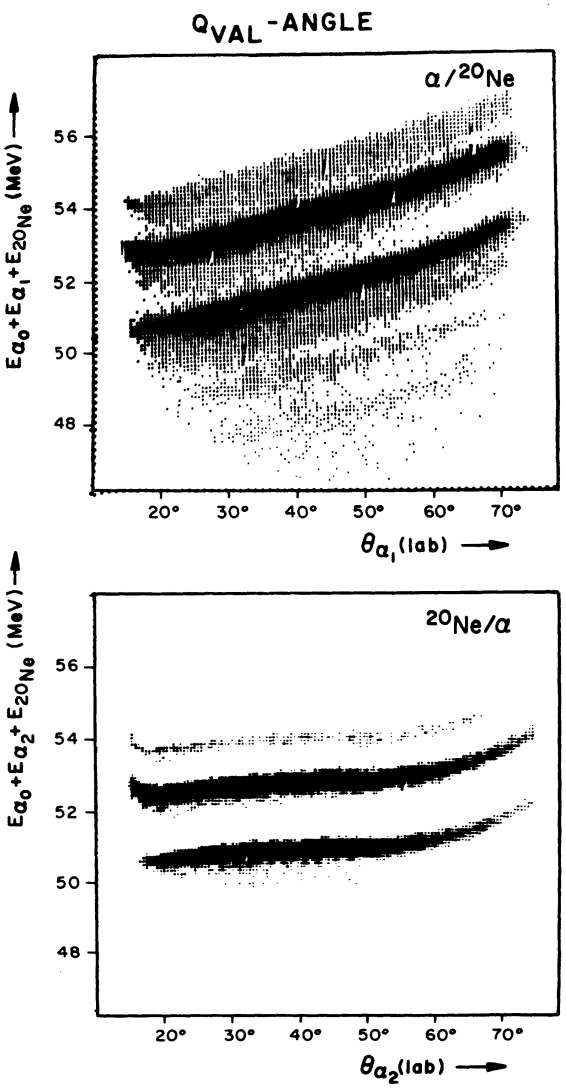

FIG. 8. Two-dimensional $Q_{val}-\theta_\alpha$ spectra for the $\alpha_0+\alpha_1+{}^{20}Ne$ final states. The three curves in each spectrum correspond to the ground, first excited (1.63-MeV), and second and third excited (4.25-4.97-MeV) states in ^{20}Ne. The nonlinearities indicated are discussed in the text.

Finally, a projection onto the mass-ratio axis of all events with Q values outside the range 45–59 MeV enabled the direct experimental determination of the shape of the background shown in Fig. 5.

4. ^{12}C channels

The identification of the $^{12}C+{}^{12}C+\alpha$ channel was complicated by the possibility of contributions from the $^{15}N+{}^{12}C+p$ channel. Since direct dE/dx particle identification was not used in the 0° detector, the corresponding mass ratios (15/12 and 12/15) would have been experimentally indistinguishable from unity, and the deduced Q_{val} would pass through the $^{12}C+{}^{12}C+\alpha$ value for $E_p=3-6$ MeV. This ambiguity was removed by examining the distribution of events in $E_1-\theta_1$ parameter space for those selected in the $M-Q_{val}$ space; no evidence was found for any such interference.

The identification of the $\alpha+{}^{12}C+{}^{12}C^*(4.43)$ channel required additional steps in the analysis in order to discriminate against contributions from background events. The excited ^{12}C channel was observed to lie above an enhanced background, the locus of which is semicircular in the region of the $^{12}C+{}^{12}C^*$ group. This region is denoted by the curves a in Fig. 7. The source of this background was found to be the detection of the four-body $^{16}O+3\alpha$ channel in which the least energetic α particle remained undetected. This conclusion was reached on the basis of an approximate computer simulation of the energy and angle distribution of the four bodies in this exit channel. A careful two-dimensional background subtraction in mass-Q-value space was performed in which the $^{12}C+{}^{12}C^*+\alpha$ events were first obtained from region c (see Fig. 7) and the events in the region between curves b and c were used for background subtraction. The $^{12}C+{}^{12}C^*+\alpha$ events were then further limited to a region in $\theta_1-\theta_2$ space corresponding to the allowed kinematic range for these events. The ratio of the $^{12}C+{}^{12}C^*+\alpha$ events remaining after background subtraction to the number of background events was 1.0. The net yield of $^{12}C+{}^{12}C^*+\alpha$ events is about one sixth the number of those observed for $^{12}C+{}^{12}C+\alpha$. Given the nature of the background subtraction, this ratio $R=\frac{1}{6}$ represents a *lower* limit on the actual ratio of the two groups of ^{12}C events.

This value for the ratio $R\geq\frac{1}{6}$ may be compared with the *upper* limit $R\leq\frac{1}{10}$ reported in Ref. 9. In attempting to account for this apparent discrepancy, the following differences between the present experiment and that of Ref. 9 may be noted where

we use the notation, quantity = (Yale, Brookhaven): E_{lab} ^{16}O = (58.3, 56.0) MeV; lab angle subtended by the PSD's = (15–75°, 20–65°); maximum observable excitation in ^{24}Mg = (~31, ~28) MeV. Although it is difficult to make a quantitative estimate of the consequences of these differences in experimental configuration, we note that all of these differences are in a direction expected to produce a relative increase for the present experiment of the observed $^{12}C + ^{12}C^* + \alpha$ yield. It is therefore unnecessary to conclude that the respective experimental results are in contradiction.

5. ^{16}O-2α channels

With the present detector arrangement, it is difficult to assess precisely the yield of ^8Be in the $\alpha_0 + ^{16}O + 2\alpha$ channel. The lifetime of the ^8Be ground state ($\tau = 2.6 \times 10^{-16}$ sec) is such that it decays into two α particles ($Q = 0.094$ MeV) while still in the vicinity of the target. With the half-angle of the decay restricted to $\theta_{lab} \leq 7°$, an estimate of roughly 60% is made for the efficiency of detecting a ^8Be moving toward a PSD. However, a competing source of events is the detection in one PSD of two α particles associated with a four-body channel independent of ^8Be, as for example

$$^{16}O + ^{12}C \rightarrow ^{16}O + 3\alpha \quad \text{(direct breakup)} \qquad \text{(a)}$$

or

$$^{16}O + ^{12}C \rightarrow \alpha_0 + ^{24}Mg^* \hookrightarrow \alpha_1 + ^{20}Ne^* \hookrightarrow \alpha_2 + ^{16}O. \qquad \text{(b)}$$

Detection of such events can contribute to the peaks in the mass-ratio spectrum observed at the values $\frac{2}{1}$ and $\frac{1}{2}$. Such events are also expected to cause an additional broadening of the mass-ratio peak depending on the relative center-of-mass energy of the two α particles. There is no evidence in the present work that the peaks in the mass-ratio spectrum correspond to $^8Be + ^{16}O$ as opposed to ^{16}O and two uncorrelated α particles. [In fact, calculations to be described in Sec. V indicate that for a statistical compound-nucleus reaction mechanism, the former is a much weaker process compared to reaction (b) above.] If the detection of ^8Be is to be of prime importance, then a completely different detector system must be used with much smaller solid angles or involving separate detection of both α particles from the decay of ^8Be. We note that the lack of any yield with a mass ratio of ~$\frac{1}{2}$ in the results of Ref. 9 originates most probably from the smaller active area of the PSD's used (4 mm × 50 mm in Ref. 9, vs 7 mm × 50 mm in the present work) and from the consequently reduced efficiency for the simultaneous detection of two α particles.

IV. PRESENTATION OF RESULTS

All the triple-coincidence events measured in this experiment were subjected to the various one- and two-dimensional time, mass-ratio, Q-value, and θ_{PSD} gates described in Sec. III B, and then analyzed with respect to the energy of the α particle detected at 0°. Provided that this α particle comes from the decay of the ^{28}Si compound system its energy bears a direct relation to the excitation energy in an intermediate ^{24}Mg system: if the reaction proceeds through given sharp states in ^{24}Mg, sharp peaks then appear in the E_{α_0} spectrum, while if the reaction proceeds through broad states in ^{24}Mg, or not through the ^{24}Mg system at all, no such sharp structure would be expected to appear.

The α-particle energy spectra measured at 0° are shown in Figs. 9 and 10 for the various reaction channels. The spectra for $^{20}Ne + \alpha_0 + \alpha_1$ in Fig. 9 show sharp individual groups indicative of the intermediate formation of discrete states in ^{24}Mg. The structureless $^{16}O + 2\alpha + \alpha_0$ and $^{12}C + ^{12}C^* + \alpha_0$ spectra in Fig. 10 offer no such indication of the participation in the interaction of sharp states in ^{24}Mg within the low statistical accuracy present.

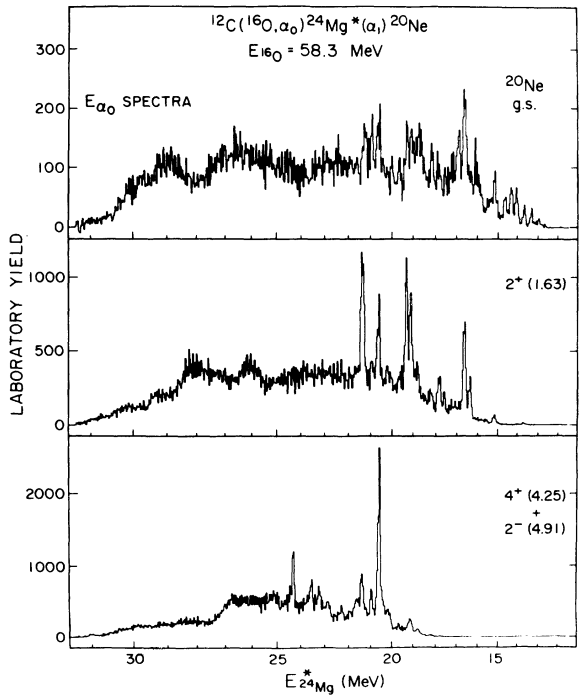

FIG. 9. Energy spectra of α particles α_0 observed at ~ 2° lab in coincidence with an α_1-^{20}Ne pair in the two position-sensitive detectors. The abscissa is plotted as excitation energy in the intermediate ^{24}Mg nucleus.

There is, however, clearly marked structure in the $^{12}C+^{12}C+\alpha$ spectrum; its interpretation is the subject of further analysis to be described below.

A. $^{20}Ne+\alpha_0+\alpha_1$ channels

Figure 11 displays the two-dimensional $\theta_1 - E^*$ (^{24}Mg) spectra for three-body final states leading to the ground, first excited (1.63-MeV 2^+), and second and third excited (4.25-MeV 4^+; 4.91-MeV 2^-) states (unresolved) of ^{20}Ne, respectively. Shown below each two-dimensional spectrum is the one-dimensional projection of events along the E^* (^{24}Mg) axis. Population of higher excited states in ^{20}Ne was not observable, since these states are unbound against α-particle decay to ^{16}O, with lifetimes much shorter than the target-to-detector flight times. The events forming straight vertical lines correspond to the observation of intermediate states in ^{24}Mg through detection at 0° of the (primary) α particle which populates the particular state in ^{24}Mg together with the detection in the PSD's of the α-^{20}Ne pair depopulating this state. The events forming the sloping loci, on the other hand, correspond to the detection at 0° of the (secondary) α particle which depopulates a state in ^{24}Mg, while the α particle which populated the state in ^{24}Mg is observed in a position-sensitive detector in coincidence with the remaining ^{20}Ne particle. The assignment of an excitation energy in ^{24}Mg in this figure is, of course, made on the assumption that the α particle detected at 0° is the α particle which populates the state in ^{24}Mg. Kinematic analysis of the events in the sloping lines allows the assignment of the corresponding excitation energy in ^{24}Mg which is in fact much smaller than the excitation energy given by the intersection of the sloping lines with the abscissa. The kinematic re-

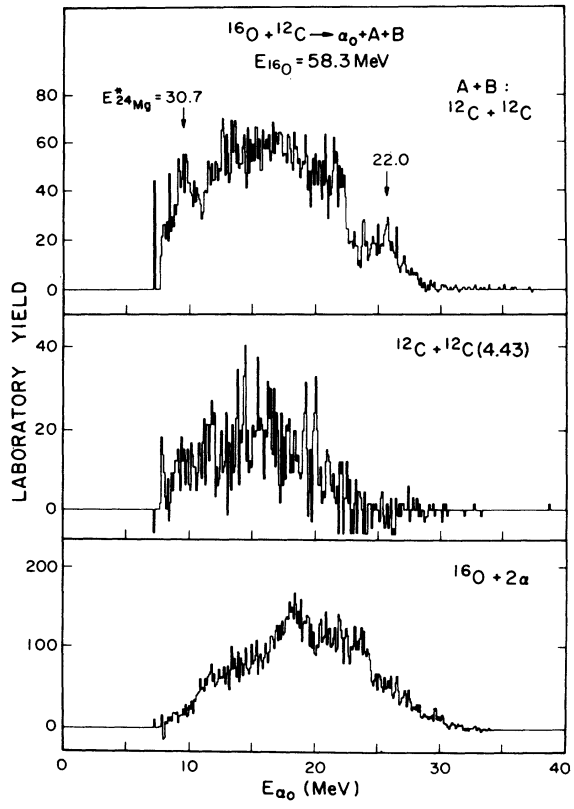

FIG. 10. Energy spectra of α particles α_0 at ~ 2° lab in coincidence with the indicated $A+B$ pair detected by the two position-sensitive detectors.

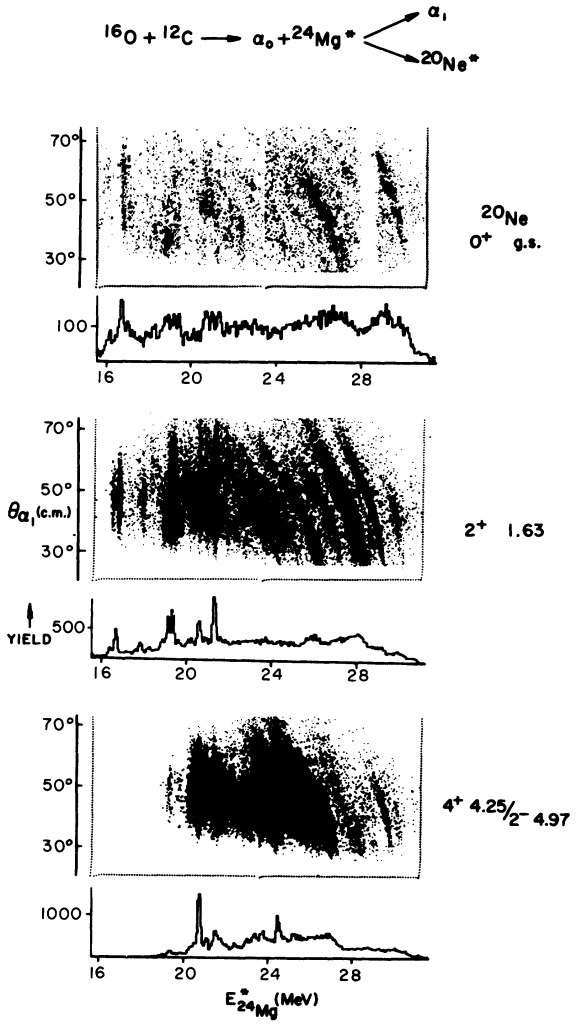

FIG. 11. α_0-α_1 angular correlations for the three $\alpha_0+\alpha_1+^{20}Ne$ channels displayed as a continuous function of excitation energy in ^{24}Mg. $E^*(^{24}Mg)$ has been calculated on the assumption that the α particle observed at 2° is from the decay of the ^{28}Si system. The straight vertical lines correspond to the detection of a primary α particle at 0°, while the curved lines indicate detection of a secondary α particle at 0°.

lationships for primary and secondary α particles are illustrated schematically in Fig. 12. The clear recognition in Fig. 11 of the two classes of events, primary and secondary, observed by this detection system will have important consequences in explaining the observed yields. This will be discussed in Sec. V C.

B. $^{12}C + ^{12}C + \alpha$ channel

We begin by noting the definite peaks in the $\alpha_0 + ^{12}C + ^{12}C$ spectrum (Fig. 10) corresponding to excitation energies of 22.0 and 30.7 MeV in ^{24}Mg. Our initial interpretation[8] of this structure was that it constituted evidence for ^{12}C-^{12}C quasimolecular configurations. However, a subsequent and more detailed investigation of the mechanisms through which this particular three-body final state may be populated has shown this interpretation to be incorrect. (See note added in proof in Ref. 8.) The source of the structure in the 0° α-particle energy spectrum shown in Fig. 10 becomes apparent in the two-dimensional spectrum shown in Fig. 13. The yield is plotted here against the relative kinetic energies of the α particle with respect to each of the ^{12}C ions observed in the PSD's. The presentation of data in this form was motivated by the methods introduced by Dalitz.[15] The axes are labeled in terms of the corresponding excitation energy in ^{16}O.

Evidence for the participation of intermediate states in ^{24}Mg (through strong correlations between the two ^{12}C ions) would appear as events lying along diagonal loci in this spectrum and as peaks in the one-dimensional spectrum in Fig. 10. The apparent absence of such diagonal lines in Fig. 13 indicates that if such states are present in this region of excitation in ^{24}Mg they are either very weakly populated or have such large decay widths as to be obscured by their overlap with other states in the surrounding continuum. Rather, the pattern of events in Fig. 13 suggests two broad orthogonal lines, each lying approximately parallel to an axis. This indicates a strong α-^{12}C correlation or final-state interaction corresponding to an excited state in ^{16}O.

There are indications of two types of structure along the bands of correlated events in Fig. 13: (1) a broad minimum appears near 12 MeV in each band; and (2) the bands are modulated by a series of narrow maxima running approximately at a 45°

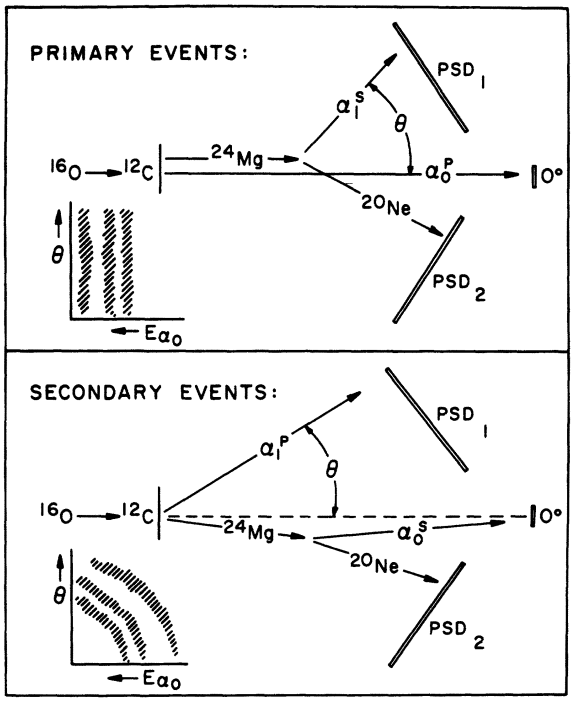

FIG. 12. Schematic interpretation of the structure observed in the experimental angular-correlation data (Fig. 11). The α particles are subscripted according to the detector in which they are observed. The superscripts P and S denote primary and secondary α particles, respectively. "Primary" refers to an α particle coming from the decay of the ^{28}Si compound system.

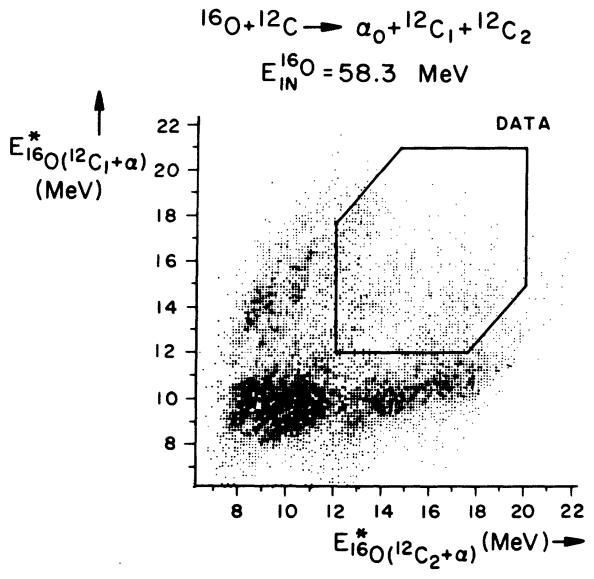

FIG. 13. Energy correlation of events in the $\alpha_0 + ^{12}C + ^{12}C$ channel. From the measured kinematic variables, the kinetic energy of the α particle relative to each ^{12}C ion has been calculated for each event. These values are then converted to an equivalent excitation energy in the ^{16}O system and used as coordinates in plotting the event. Only channels with two counts or more are displayed.

angle to the axes. This structure can be understood with the aid of Fig. 14, which represents a kinematic mapping of the parameter space shown in Fig. 13 using a two-step sequential reaction model shown in the figure inset. The contours of kinematic lines for events corresponding to the indicated scattering angles are shown in Fig. 14 for the sequential decays. It may be noted that the direction of the structure in the data coincides with the isoangle contours associated with the first step of the reaction.

In order to check this interpretation against the experimental data and to obtain a better qualitative picture of the characteristic angular distributions for the $^{16}O + ^{12}C$ scattering and the subsequent ^{16}O decay, a series of Monte Carlo simulations of a two-step sequential reaction were made. The two angular distributions mentioned above were parametrized under various assumptions and used to weight scattering events randomly selected in the appropriate center-of-mass systems. The following effects were considered in the Monte Carlo calculations: the resolution, nonlinearities, and thresholds in the position and energy determinations, the finite solid angle of the detector at 0°, and the width of the excited state in ^{16}O. The amplitudes for the observation of the recoil ^{12}C ion (from the first step of the reaction) in each of the PSD's were added incoherently, this approximation being valid when the experimental energy resolution is much greater than the natural width of the excited ^{16}O nucleus.

It is clear from Fig. 14 that an intensified yield may be expected in the region of the data where the orthogonal lines cross, not only because of the addition of the intensities from the crossing bands, but also because of the smaller spacing between the isoangle lines. The sizes of these enhancements were first isolated and studied through Monte Carlo calculations employing isotropic angular distributions (in the center-of-mass systems). In subsequent calculations the angular distribution for θ_{34} (see Fig. 14) was varied while that for θ_{56} remained isotropic. This assumption of isotropy for θ_{56} is consistent both with the experimental results and the fact that all of the magnetic substates of an excited state in $^{16}O^*$ may be populated at the scattering angles considered here, $45° \leq \theta_{34} \leq 140°$.

The results of a Monte Carlo simulation for an excited state in ^{16}O at 10 MeV are shown in Fig. 15. The simulation qualitatively reproduces the data and demonstrates that a two-step reaction proceeding through an excited state in ^{16}O can account for the type of structure indicated in Fig. 13. Furthermore, when the spectrum of α particles at ~0° is obtained from the simulation, two peaks appear at approximately the energies indicated by the arrows in Fig. 10. The angular distribution for θ_{34} used in the simulation is peaked forward of 90° c.m. in the region 50 → 60°. About 35% of the total yield in the observed region of 50 to 130° occurred at angles larger than 90° c.m. and the spacing between maxima in the angular distribution was 15–20°.

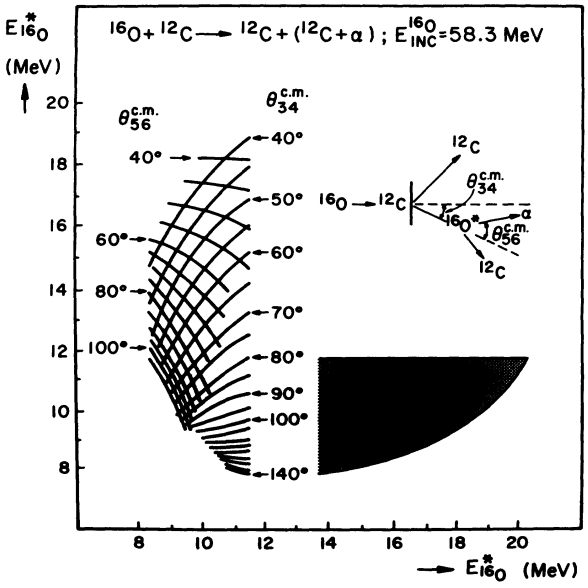

FIG. 14. A kinematic mapping of the parameter space shown in Fig. 13, based on the two-step reaction $^{12}C(^{16}O, ^{12}C)^{16*}O(\alpha_0)^{12}C$.

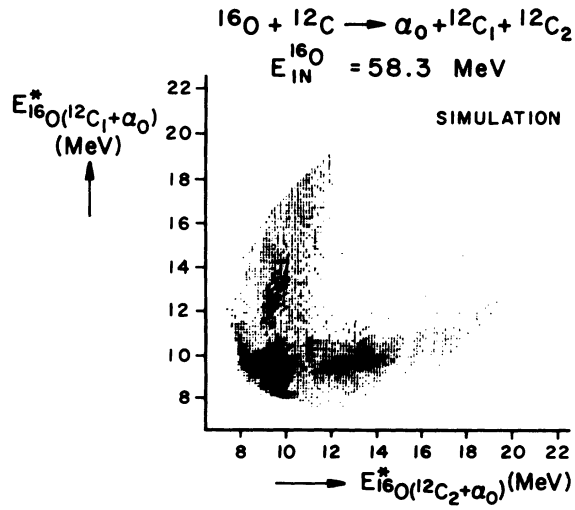

FIG. 15. A Monte Carlo simulation of the reaction $^{12}C(^{16}O, ^{12}C)^{16*}O(\alpha)^{12}C$ for $E^*_{^{16}O} \sim 10$ MeV. A slight nonlinearity in the energy calibration of the PSD's included in this calculation is responsible for the over-all sloping of the kinematic lines away from the coordinate axes at high excitation.

There are a number of excited states in ^{16}O in the region 8.5–10.5 MeV excitation which (individually or collectively) could be responsible for the structure in Fig. 13. The smearing of the structure in Fig. 13 over a width of approximately 1.5 MeV excitation in ^{16}O is consistent with the finite position and energy resolution of the three detectors. This experimental width and the slight nonlinearity do not permit more precise identification of the state or states in the region 8.5–10.5 MeV responsible for the structure. However, it is known from measurements at higher ^{16}O bombarding energy (i.e., 65 MeV,[16] 67 MeV[17]) that the 10.34-MeV 4^+ state in $^{16}O^*$ is strongly excited in the $^{12}C(^{16}O, ^{12}C)^{16}O^*$ reaction and this state is therefore a most probable candidate.

There is significant $^{12}C + ^{12}C + \alpha$ yield in the area of Fig. 13 corresponding to an excitation in $^{16}O^*$ of 12 MeV or greater along each axis. It is not possible to ascertain whether this yield arises from the population of close-lying states in $^{16}O^*$ at higher energies, from a direct breakup of the ^{16}O projectile, or from compound-nucleus formation and decay. Each of these processes could account for the lack of structure in the region $E^*(^{16}O) > 12$ MeV. This yield will be the subject of further discussion in Sec. V.

C. $^{12}C + ^{12}C^* + \alpha$ channel

Figure 16 exhibits the corresponding α-^{12}C correlation spectrum for the excited ^{12}C three-body final state. The background has been subtracted as described in Sec. III B 4 above. The right-hand ordinate is approximately scaled for α particles correlated with the ground-state ^{12}C nucleus; the left-hand ordinate is scaled for α particles correlated with the ^{12}C nucleus excited to its 4.43-MeV (2^+) level. No evidence is seen for any such correlations nor for correlations between the two ^{12}C nuclei; rather, the distribution is suggestive of a phase-space population confined within the ellipsoidal boundaries determined by the kinematics and detector thresholds for energy and angle.

D. $^{16}O + 2\alpha + \alpha$ channels

Because of the ambiguities introduced by the contributions from the four-body final states, no information is expected from further consideration of these channels. Indeed, analyses of the data along the lines described in the preceding sections offered no indication for any unusual structure or correlations.

E. Section summary

The measurements described in this section represent a detailed comparison of the most important three-body exit channels involved in the $^{16}O + ^{12}C$ reaction. Evidence has been presented that the $^{20}Ne + \alpha + \alpha$ channels carry away approximately 90% of the three-body flux at a bombarding energy $E_{^{16}O} = 58.3$ MeV. The four-body background was found to contribute almost 50% of the total number of triple-coincidence events measured. No evidence was found for the population of sharp states in ^{24}Mg of ^{12}C-^{12}C molecular structure. Rather, the $^{12}C + ^{12}C + \alpha$ channel was found to be dominated by an intermediate state(s) in ^{16}O at ~10 MeV excitation which decays into an α particle and one of the ^{12}C nuclei.

The discussion in this section has centered around a consideration of the reaction mechanisms involved in the particular scattering channels observed in this experiment. With the understanding of the $^{12}C + ^{12}C + \alpha$ yield as described in Sec. B above, it is possible to exclude from this yield those events which arise from the population and decay of the ~10-MeV state in $^{16}O^*$ and to focus on the remaining α-^{12}C-^{12}C data within the framework of a statistical model for nuclear reactions. In the following section, a comparison of predictions obtained with the Hauser-Feshbach statistical model will be made with the corresponding experimental yields from the ^{12}C and ^{20}Ne three-body channels.

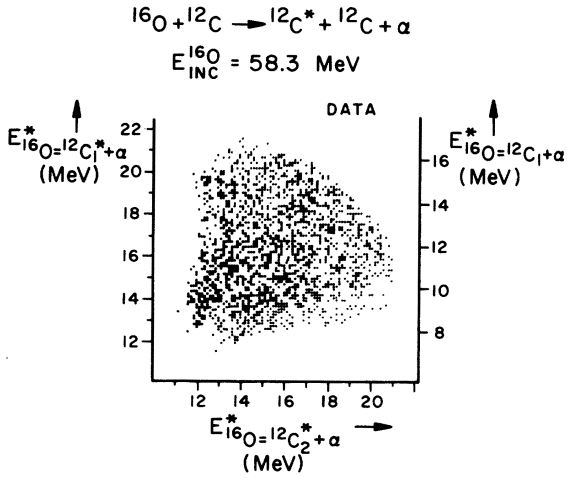

FIG. 16. Two-dimensional spectrum of events in the $\alpha_0 + ^{12}C + ^{12}C^*$ channel plotted as a function of the relative kinetic energy of each α-^{12}C pair. The coordinates of each event were obtained as described in Fig. 13. The scale of the left-hand ordinate is appropriate for those events in which the α particle is associated with the ^{12}C nucleus excited to its 4.43-MeV (2^+) level; the right-hand ordinate, for those α particles correlated with the ground state ^{12}C.

V. STATISTICAL MODEL ANALYSES

A. Introduction

The statistical model of nuclear reactions[18] has met with much success in predicting individual channel reaction cross sections in the $^{16}O + ^{12}C$ and $^{12}C + ^{12}C$ reactions at intermediate energies.[19,20] Thus it is natural to ask to what extent such a model can account for the gross properties of the yields measured in the three-body channels described in the previous section.

While the ^{12}C channels were seen to proceed primarily through a direct interaction involving a ^{12}C and an α particle, a number of scattering events in this channel are not necessarily so associated. These events lie in the kinematic region of Fig. 13 bounded by $E^* > 12$ MeV in ^{16}O. There is no strong evidence for any intermediate α-^{12}C interaction here, although this process is not ruled out. The formation and decay of ^{24}Mg could then account for a sizable fraction of these events and a comparison with the statistical model is thus meaningful.

Recent calculations by several workers[21] have demonstrated that the energy-averaged cross sections of a number of high-spin states observed in the $^{12}C(^{16}O, \alpha)^{24}Mg$ reaction are consistent with a purely statistical compound-nucleus process. The associated α-particle energy spectra exhibit peaks superimposed on a smooth background of events which also presumably arise from the population of states of a statistical compound nature, though of low spin and, hence, with a high level density. Thus it is possible that a comparison of the ratio of theoretical and experimental yields averaged over excitation energy in an assumed intermediate ^{24}Mg compound system for the three ^{20}Ne and two ^{12}C channels may give some information on the source of the observed ^{12}C three-body yield in the kinematic region mentioned above.

Furthermore, the two-step sequential processes involved here in the ^{20}Ne channels and possibly in the ^{12}C channels as well should provide a valuable check on the statistical parameters describing the coupled compound nuclear systems ^{28}Si and ^{24}Mg.

B. Angle-integrated experimental yields

The data for the three-body channels involving ^{12}C in the final state were taken from the region of the spectrum enclosed by the full curve shown in Fig. 13. Events lying outside this region were excluded from consideration. The data from the inelastic $^{12}C^*$ three-body channel were taken as the entirety of those shown in Fig. 16. The data for the ^{20}Ne final states were taken from the spectra shown in Fig. 11.

The yield extracted for a given α-particle angle ($\bar{\theta}$) and excitation energy interval (ΔE^*) in ^{24}Mg is related to the associated triple differential cross section for a particular channel by the re-

TABLE I. Statistical-model parameters.

Optical-model parameters

System	V_{real} (MeV)	R (fm)	a (fm)	W (MeV)	R (fm)	a (fm)	Ref.
$^{12}C + ^{12}C$	14	6.18	0.35	$0.4 + 0.1E$	6.41	0.35	26
$^{20}Ne + \alpha$	57.5	5.3	0.56	13.2	5.30	0.56	27
$^{16}O + ^{8}Be$	14	6.1	0.49	$0.4 + 0.15E$	6.10	0.49	
$^{23}Na + p$	$56 - 0.55E$	3.56	0.65	13.5	3.56	0.47	28
$^{23}Mg + n$	$48.2 - 0.3E$	3.56	0.65	11.5	3.55	0.47	28
$^{16}O + ^{12}C$	17	6.49	0.49	$0.4 + 0.1E + 0.006E^2$	6.11	0.15	26
$^{24}Mg + \alpha$	54.4	4.9	0.53	9.8	4.90	0.53	27
$^{20}Ne + ^{8}Be$	14	6.36	0.49	$0.4 + 0.15E$	6.36	0.49	
$^{27}Al + p$	$52.2 - 0.3E$	3.75	0.65	11.5	3.75	0.47	28
$^{27}Si + n$	$48.2 - 0.3E$	3.75	0.65	11.5	3.75	0.47	28

Level-density parameters (Ref. 25)

$$\rho(E,J) = \frac{(2J+1)}{12a^{1/4}(U+t)^{5/4}(2\sigma^2)^{3/2}} \exp[2(aU)^{1/2}] \exp\left[\frac{-(J+\frac{1}{2})^2}{2\sigma^2}\right],$$

where $U = E - \Delta$, $\sigma^2 = \mathcal{I}t/\hbar^2$, $U = at^2 - t$, $\mathcal{I} = \frac{2}{5}MR^2(1 + 0.31\beta + 0.44\beta^2)$, and $R = r_0 A^{1/3}$. $a = 0.149A$, $\Delta = 3.6$ for even-even nuclei; $r_0 = 1.2$ fm, $\Delta = 1.8$ for odd-even nuclei; $\beta = 0.3$, $\Delta = 0.0$ for odd-odd nuclei.

lationship

$$Y(\bar{\theta}_0, \bar{\theta}, E^*) \propto \frac{d^3\sigma}{d\Omega_0 d\Omega_{\mathrm{PSD}} dE^*} F(\bar{\theta}_0) F(\bar{\theta}_{\mathrm{PSD}}) \times \overline{\Delta\Omega}_0 \overline{\Delta\Omega}_{\mathrm{PSD}} \Delta E^*, \quad (1)$$

where laboratory quantities are indicated by superposed bars and where the function F is the appropriate transformation between center-of-mass and laboratory coordinate frames. The appropriate experimental quantity with which model calculations are to be compared is the angle-integrated double differential cross section in the center-of-mass system

$$\frac{d^2\sigma(E^*)}{d\Omega_0 dE^*} = \int_{\Delta\Omega_{\mathrm{PSD}}} \frac{d^3\sigma}{d\Omega_0 d\Omega_{\mathrm{PSD}} dE^*} d\Omega_{\mathrm{PSD}}, \quad (2)$$

where the integration is performed over the angular range kinematically available to the particular channel at a given excitation energy E^*.

The resultant experimental cross sections, not possessing an absolute normalization but normalized relative to one another, will be displayed in a later section together with the corresponding model predictions.

C. Hauser-Feshbach calculations

The basic assumption involved in these calculations, as noted above, is that the individual channels proceed through two-step sequential processes involving compound nuclear states in ^{28}Si and ^{24}Mg.

The calculations were performed using the computer codes STATIS and BRKUP .[22] As input parameters, these codes required the transmission coefficients for all the important exit channels coupled to the two compound systems. These were obtained from optical-model calculations using the code ABACUS [23] with optical-potential parameters derived from the literature. The existence of a consistent set of such parameters for the heavy-ion channels was particularly useful, these being obtained partly from the results of previous elastic scattering measurements done at this laboratory.[24] The calculations were made for the channels indicated in Table I at center-of-mass energy intervals of 1.0 MeV using the potential parameters also indicated there. The parameters used in the level-density expression within the Hauser-Feshbach model are given in the table and were obtained by comparison of calculated Hauser-Feshbach cross sections with the ^{12}C(^{16}O, α)^{24}Mg reaction data of Halbert, Durham, and van der Woude.[19]

The calculations were of two types depending on whether the particular α particle detected at 0° came from the decay of ^{28}Si (= primary reaction) or from the subsequent decay of ^{24}Mg (= secondary reaction). The relative contributions of these two processes can be clearly seen in the data shown in Fig. 11. The ^{12}C channels required only the calculation of the primary contribution, while the ^{20}Ne channels required the sum of the primary and secondary contributions in order to arrive at a valid comparison with the experimental cross sections.

Calculations of primary cross sections. For the primary case, the cross section is given by the expression

$$\frac{d^3\sigma(\theta_1, \theta_2, E^{*\prime}, I')}{d\Omega_1 d\Omega_2 dE^*} = \sum_I \frac{d\sigma}{d\Omega_1}(E^*, \theta_1, I) \times \rho(E^*, I) \frac{dB}{d\Omega_2}(E^*, I, \pi \to E^{*\prime}, I', \pi'), \quad (3)$$

where $\theta_1 = 0°$ and $\pi = (-1)^I$ since only normal-parity states are populated in ^{24}Mg when the primary α particle is detected along the beam axis. $(d\sigma/d\Omega)(E^*, \theta_1, I)$ is the differential cross section for formation of a state in ^{24}Mg of spin I at an excitation energy E^* and $\rho(E^*, I)$ is the level density of ^{24}Mg for states of normal parity. Expressions for the cross section $d\sigma/d\Omega_1$ are given, e.g., in Ref. 18. $dB/d\Omega_2$ is the differential branching ratio for emission of a second particle from an $m = 0$ substate in ^{24}Mg leading to a given state $(E^{*\prime}, I', \pi')$ in ^{20}Ne or ^{12}C, and is given by

$$\frac{dB}{d\Omega} = \frac{1}{4\pi(2I+1)} \sum_L \sum_{l's'} T_{l'}(E^{*\prime}) \bar{Z}(I, I, I, I; 0, L) \bar{Z}(l', I, l', I; s', L)(-1)^{s'} \frac{P_l(\cos\theta_2)}{\sum_{c''} T_{l''}(c'')}, \quad (4)$$

where $s' = I' + i'$, I' and i' are the spins of the decay products, and $I = l' + s'$. $\bar{Z}$ is the z coefficient defined in Ref. 18 and T_l is an optical-model transmission coefficient. $\sum_{c''} T_{l''}(c'')$ represents the total number of open channels available for the decay of the particular state in ^{24}Mg. Evaulation of this quantity was done using explicitly the levels of the various nuclei with known spin and parity, and a level-density formula at higher excitation energies. Yrast-level cutoffs were applied in the calculation of $(d\sigma/d\Omega)(\theta_1, E^*, I)$ and $dB/d\Omega$.

In the case of ^{24}Mg decaying into identical spin-

zero particles, special considerations apply in evaluating Eq. (4). Only states of even spin and parity in ^{24}Mg may undergo such decay, and the summation over l' is restricted to even values. Symmetrization of the wave function and the indistinguishability of the particles require that the quantity $dB/d\Omega$ be multiplied by a factor of 4. For the decay of ^{24}Mg into ^{12}C + ^{12}C*, these restrictions on the states in ^{24}Mg or on the values of l' do not apply. The position-sensitive detectors, however, do not distinguish between ^{12}C and ^{12}C*, and $dB/d\Omega$ must be multiplied by a factor of 2. These above conditions also apply in evaluating angle-integrated cross sections, provided that the integration does not go beyond 90° center of mass. This was the case in both the calculations and analysis of the data.

Calculation of secondary cross sections. In this case the intermediate ^{24}Mg system is not constrained to the $m=0$ substate, and the angular distribution of the second α particle leading to ^{20}Ne is reasonably taken to be isotropic in the center of mass. The primary α particle from ^{28}Si, now detected in the angular range $15° < \bar{\theta} < 75°$, is well described by a $(\sin\theta)^{-1}$ distribution. Thus the cross section is now given by the expression

$$\frac{d^3\sigma}{d\Omega_1 d\Omega_2 dE^*}(\theta_1, \theta_2, E^{*\prime}, I') = \sum_{I\pi} \frac{d\sigma}{d\Omega}(\theta_1, E^*, I, \pi)\rho(E^*, I, \pi)\frac{B(\theta_2; E^*, I, \pi \rightarrow E^{*\prime}, I', \pi')}{4\pi}, \tag{5}$$

where $\theta_2 = 0°, 15° < \bar{\theta}_1 < 75°$,

$$B = \sum_{l's'} T_{l'}(E^{*\prime}) \Big/ \sum_{c''} T_{l''}(c''), \tag{6}$$

and

$$\frac{d\sigma}{d\Omega}(\theta_1, E^*, I, \pi) = \frac{\sigma(E^*, I, \pi)}{2\pi^2}\frac{1}{\sin\theta_1}. \tag{7}$$

Addition of the primary and secondary cross sections. The excitation energy in ^{24}Mg is defined by the energy of the primary α particle. Since it is impossible for any given event to know whether a primary or a secondary α particle is detected at 0°, an ambiguity results when attempting to present the data as a function of excitation energy in ^{24}Mg. The data presented in Fig. 11 are given in fact as a function of the energy of the α particle detected at 0°; this energy was then converted into an equivalent excitation energy in ^{24}Mg on the assumption (for purposes of presentation only) that the primary α particle was detected at 0°. In comparing the statistical-model calculations to the data, therefore, additional steps were required before the calculated secondary cross sections could be combined with the primary cross sections. For a given excitation energy in ^{24}Mg there is a unique relation between the energy and angle of the primary α particle, detected in one of the PSDs, and the energy of the secondary α particle, detected at 0°. This allows the assignment of a "pseudo"-excitation energy in ^{24}Mg for the secondary reaction, namely that excitation in ^{24}Mg which would prevail had the secondary α particle in fact been a primary α particle. Primary reactions and secondary reactions, thus combined using this pseudoexcitation energy for the secondary reaction, are compared to the data in Fig. 17.

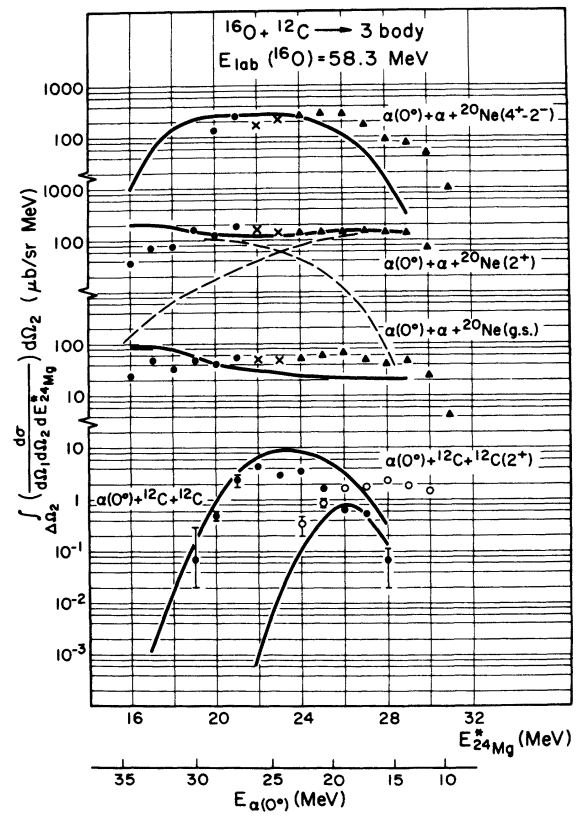

FIG. 17. A comparison of two-step statistical model calculations to the experimental data. Experimental angular distributions have been integrated over the center-of-mass angular range: 60–90° (circles); 50–90° (crosses); 40–90° (triangles). The dashed curves represent the relative primary and secondary α-particle contributions to the ^{20}Ne (2^+) channel. The data have been normalized to the ^{20}Ne (2^+) prediction. The ^{12}C + ^{12}C + α_0 data shown here are selected from the region of the kinematic plane in Fig. 13 given by $E^*(^{16}\text{O}) \geq 12$ MeV.

D. Results and conclusions

The angle-integrated data for the three ^{20}Ne channels and the two ^{12}C channels are displayed in Fig. 17 together with the results of the two-step Hauser-Feshbach calculations described in the previous section. The absolute cross sections for the data have been adjusted by normalizing the ^{20}Ne (2^+) cross sections to the predicted results. The relative contributions of the primary and secondary reactions are indicated by dashed curves for that channel in the figure.

In general, the experimental cross sections are well accounted for in this treatment. The selected ^{12}C ground-state cross sections are reasonably well reproduced in both shape and magnitude. The ^{12}C-excited channel, however, is not well reproduced particularly at higher excitation energies. This most probably results from the presence of additional flux from the breakup of ^{16}O above 11 MeV in excitation. It should be noted here that there exists another reaction route that can feed these ^{12}C channels. This is the statistical process

$$^{16}O + ^{12}C \rightarrow ^{28}Si^* \rightarrow ^{12}C + ^{16}O^*$$
$$\hookrightarrow \alpha + ^{12}C .$$

Similar Hauser-Feshbach calculations placed an estimated upper limit of 10% on their strength compared to the ^{24}Mg decay route. Hence, these contributions were not explicitly considered here.

Although the angle-integrated cross sections presented in Fig. 17 serve to illustrate the over-all relative yields for the different channels, there is considerably more information contained in the differential cross sections. These are shown in Figs. 18 and 19 for selected excitation energies in ^{24}Mg. The data represent a summation of events over a 1-MeV interval centered around the indicated values. The errors shown are based solely on counting statistics. The angular distributions show some structure which becomes less pronounced for increasing spin in ^{20}Ne. The $^{12}C + ^{12}C$ cross sections show considerable structure. Note that these cross sections show the symmetry required by the presence of identical particles.

The full-drawn curves are the results of the Hauser-Feshbach calculations described above. The agreement with experiment is reasonably good. That the data show more structure than the calculations may possibly arise from the small size of the energy interval (1 MeV of excitation in ^{24}Mg) over which the data are summed. It may be noted in Fig. 9 that the spectrum of α particles at 0° does not indicate strong states in this region of excitation which could produce such structure. However, the secondary reaction, proceeding through isolated states in ^{24}Mg at lower excitation in ^{24}Mg, is more probably responsible for some

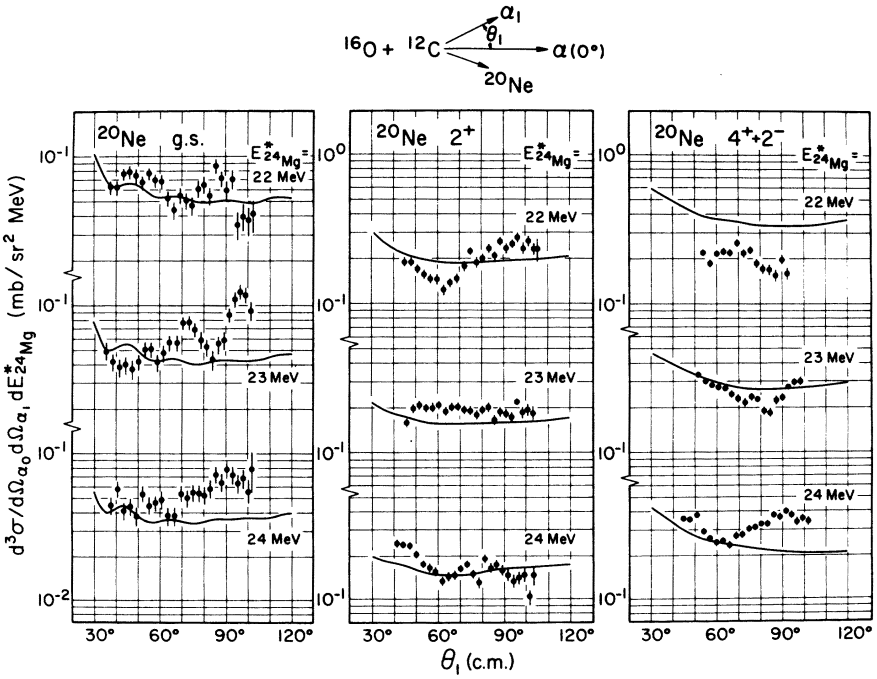

FIG. 18. α_0-α_1 angular correlations for the $\alpha_0 + \alpha_1 + ^{20}Ne$ final state. The curves are results of the Hauser-Feshbach calculations described in the text.

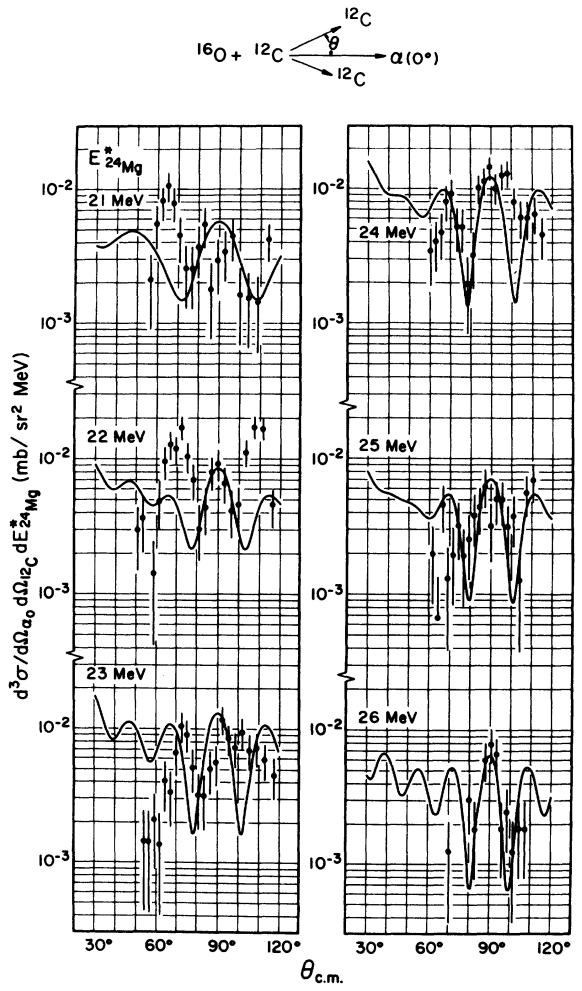

FIG. 19. α_0-^{12}C angular correlations for the $\alpha_0 + ^{12}C + ^{12}C$ channel. The data are selected from the region of the kinematic plane in Fig. 13 define by $E^*(^{16}O) > 12$ MeV. The curves are results of the Hauser-Feshbach calculations described in the text.

of the observed structure. The predominant angular momenta in ^{24}Mg contributing to the cross sections in this region are 7, 8, and 9 for ^{20}Ne, and 6 and 8 for $^{12}C + ^{12}C$. The densities of levels in ^{24}Mg at $E^* = 23$ MeV given by the level-density expression used in this calculation are 150, 70, 30, and 10 levels per MeV for spins 6, 7, 8, and 9, respectively.

The periodicity and magnitude of the pronounced structure appearing in the $^{12}C + ^{12}C$ angular distribution in Fig. 19 are reproduced rather well by the statistical-model calculations. The origin of this structure is found in the exclusion of the odd angular momenta in the decay of ^{24}Mg into two ^{12}C nuclei (and, of course, in the fact that the ^{24}Mg is initially in an $m = 0$ substate). Thus the angular distribution consists predominantly of $[P_6(\cos\theta)]^2$ and $[P_9(\cos\theta)]^2$ whereas in the case of the $^{20}Ne + \alpha$ decay, odd angular momenta also participate and smooth the angular correlations. Indeed, the over-all agreement of the statistical model predictions for the $\alpha(0°) + ^{12}C + ^{12}C$ yield as evidenced in Figs. 17 and 19 strongly suggests that the events lying in the kinematic region of Fig. 13 bounded approximately by $E^* > 12$ MeV arise predominantly from the formation and subsequent decay of ^{24}Mg into two ^{12}C nuclei.

It is interesting to note that the formation of ^{24}Mg and subsequent decay into two ^{12}C nuclei has also been observed in the ^{20}Ne(^{4}He, ^{12}C)^{12}C reaction by Lassen[29] in the region of excitation $22 < E^*(^{24}Mg) < 26$ MeV. Analysis of the angular distributions indicated the reaction proceeded predominantly through compound states with $J^\pi = 6^+, 8^+$. Thus it seems likely that the fission into $^{12}C + ^{12}C$ of the same states in ^{24}Mg has been observed although these states were populated in two different reactions, ^{20}Ne(α, ^{12}C)^{12}C and ^{16}O(^{12}C, α)^{24}Mg $\rightarrow ^{12}C + ^{12}C$. Further support of this suggestion is obtained from a comparison of the absolute cross sections measured for ^{20}Ne(α, ^{12}C)^{12}C and the corresponding statistical model prediction. This comparison is made in Fig. 20 which shows the data of Ref. 29, the average value of the fluctuating cross sections (dotted line), and the Hauser-Feshbach prediction (full line). The Hauser-Feshbach calculation employed the same parameters as used in the two-step three-body final-state calculations. The agreement is excellent.

In conclusion, the experimental results indicate that the $^{16}O + ^{12}C \rightarrow \alpha + ^{12}C + ^{12}C$ reaction proceeds primarily through a two-step process involving the formation of ^{16}O* (~10 MeV) which then decays into $\alpha + ^{12}$C. The events corresponding to the $\alpha(0°) + ^{12}C + ^{12}C^*$ (4.43-MeV) final state did not reveal any such two-step process but showed a phase-space-like distribution. All of the remaining data, viz. the $\alpha(0°) + \alpha + ^{20}$Ne channels and a selected portion of the $\alpha(0°) + ^{12}C + ^{12}C$ reaction yield, were well reproduced by a statistical model for the reaction mechanism in which the compound nuclei ^{28}Si and ^{24}Mg are formed.

No evidence was found in this three-body reaction for the existence of sharp high-spin quasi-molecular states in ^{24}Mg. We note that the quasi-molecular states seen earlier in $^{12}C + ^{12}$C-induced reactions[5,6] were not expected to be observed in this work. The reasons for this are the low angular momenta of these states, $I \leq 4$, and the fact that in the present experiments angular momentum matching favors the population of states in ^{24}Mg with higher spin. The comparison of Hauser-

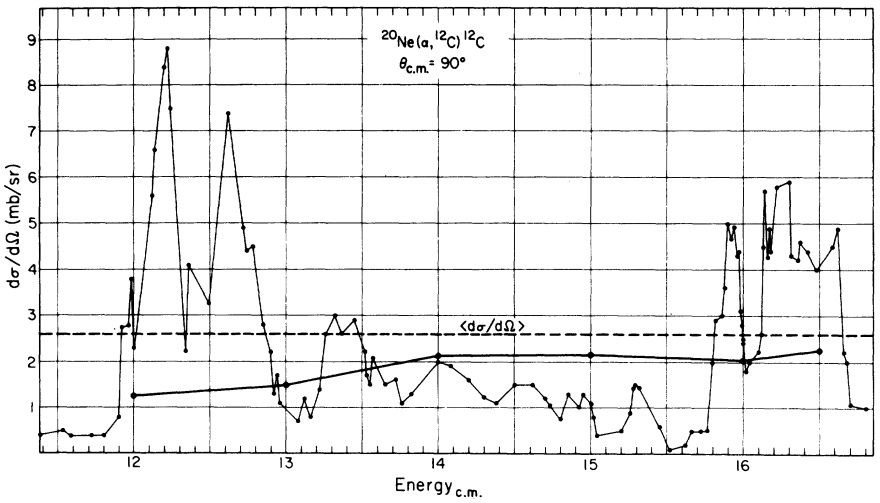

FIG. 20. Comparison of the $^{20}Ne(\alpha, ^{12}C)^{12}C$ reaction at $\theta_{c.m.} = 90°$ from Ref. 29 and the predictions of the Hauser-Feshbach statistical theory. The calculations, performed at 1-MeV intervals, are connected by a full drawn line. The energy average of the experimental cross section is given by the dotted line.

Feshbach calculations with the data suggests that we have observed the formation of ^{24}Mg in the $^{12}C(^{16}O, \alpha)^{24}Mg$ reaction and its subsequent decay into $^{12}C + ^{12}C$. This process, however, involves overlapping statistical compound states in ^{24}Mg with $J^{\pi} \sim 6^+ - 8^+$ rather than the molecular-type states originally sought in this experiment.

ACKNOWLEDGMENTS

The participation of Dr. Paulo Maurenzig in some aspects of this work is gratefully acknowledged. The technical assistance of Kenzo Sato, C. E. L. Gingell, and Dr. Edith Fehr was essential to its success.

---

*Work supported by the U. S. Atomic Energy Commission under Contract No. AT(11-1)-3074.

†Current address: Kellogg Radiation Laboratory, California Institute of Technology, Pasadena, California 91109.

‡Current address: Gesellschaft für Schwerionenforschung, Darmstadt, West Germany.

[1]R. Middleton, J. D. Garrett, and H. T. Fortune, Phys. Rev. Lett. 24, 1436 (1970).

[2]A. Arima, V. Gillet, and J. Ginocchio, Phys. Rev. Lett. 25, 1043 (1970).

[3]A. Gobbi, P. R. Maurenzig, L. Chua, R. Hadsell, P. D. Parker, M. W. Sachs, D. Shapira, R. Stokstad, R. Wieland, and D. A. Bromley, Phys. Rev. Lett. 26, 396 (1971).

[4]D. P. Balamuth, J. E. Holden, J. W. Noé, and R. W. Zurmühle, Phys. Rev. Lett. 26, 1271 (1971); R. W. Zurmühle, D. P. Balamuth, L. K. Fitfield, and J. W. Noé, *ibid.* 29, 795 (1972).

[5]E. Almqvist, D. A. Bromley, and J. A. Kuehner, Phys. Rev. Lett. 4, 515 (1960).

[6]J. R. Patterson, H. Winkler, and C. S. Zaidins, Astro-Phys. J. 157, 367 (1969).

[7]E. Almqvist, D. A. Bromley, J. A. Kuehner, and B. Whalen, Phys. Rev. 130, 1140 (1963).

[8]D. A. Bromley, L. Chua, A. Gobbi, P. R. Maurenzig, P. D. Parker, M. W. Sachs, D. Shapira, R. G. Stokstad, and R. Wieland, J. Phys. (Paris) 32, C6-5 (1971).

[9]M. J. LeVine, D. Schwalm, and M. G. Littman, J. Phys. (Paris) 32, C6-219 (1971).

[10]E. Heinicke and H. Baumann, Nucl. Instrum. Methods 74, 229 (1969).

[11]*Guide to the Detection and Use of Position Sensitive Detectors*, edited by W. W. Daehnick; Nuclear Diodes, Inc., Prairie View, Ill.

[12]J. Birnbaum and M. W. Sachs, Phys. Today 21, 43 (1968).

[13]L. C. Northcliffe and R. F. Schilling, Nucl. Data A7, 233 (1970).

[14]S. B. Kaufman, D. B. Wilkins, M. J. Fluss, and E. P. Steinberg, Nucl. Instrum. Methods 82, 117 (1970).

[15]R. H. Dalitz, Rep. Progr. Phys. 20, 163 (1957).

[16]W. von Oertzen, H. G. Bohlen, H. H. Gutbrod, K. D. Hildenbrand, U. C. Voos, and R. Bock, in *Proceedings of the International Conference on Nuclear Reactions Induced by Heavy Ions*, Heidelberg (North-Holland, Amsterdam, 1970), p. 297.

[17]P. D. Parker, private communication.

[18]H. Feshbach, in *Nuclear Spectroscopy* (Academic, New York, 1960), Part B, p. 625.

[19]M. L. Halbert, F. E. Durham, and A. van der Woude, Phys. Rev. 162, 899 (1967).

[20]E. Almqvist, J. A. Kuehner, D. McPherson, and E. W. Vogt, Phys. Rev. 136, B84 (1964); J. P. Bondorf and R. B. Leachman, K. Dan. Vid. Selsk. Mat. Fys. Medd. 34, (No. 10) (1965); J. Bondorf, Nucl. Phys. A202, 30 (1973).

[21]L. R. Greenwood, K. Katori, R. E. Malmin, T. H. Braid, J. C. Stoltzfus, and R. H. Siemssen, Phys. Rev. C 6, 2112 (1972); R. G. Stokstad, D. Shapira, L. Chua, A. Gobbi, P. D. Parker, M. W. Sachs, R. Wieland, and D. A. Bromley, Bull. Am. Phys. Soc. 17, 529 (1972).

[22]R. G. Stokstad, Wright Nuclear Structure Laboratory, Yale University Internal Report No. 52, 1972 (unpublished).

[23]E. H. Auerbach, computer code ABACUS-2, Brookhaven National Laboratory, 1964 (unpublished).

[24]W. Reilly, R. Wieland, A. Gobbi, M. W. Sachs, and D. A. Bromley, Nuovo Cimento 13A, 913 (1973).

[25]D. W. Lang, Nucl. Phys. 42, 353 (1963).

[26]A. Gobbi, in Proceedings of the Symposium on Heavy Ion Scattering, Argonne National Laboratory, March 1971, edited by R. H. Siemssen, ANL Report No. ANL-7837 (unpublished), p. 63.

[27]G. R. Satchler, Nucl. Phys. 70, 177 (1965).

[28]F. G. Perey, Phys. Rev. 131, 745 (1963).

[29]N. O. Lassen, Phys. Lett. 1, 65, 161 (1962); N. O. Lassen and J. S. Olsen, K. Dan. Vidensk. Selsk. Mat.-Fys. Medd. 33, 1 (1963).